Electronic Supporting Information

Design of Fe and Cu bimetallic integration on Nitrogen-containing microporous graphene-like carbon via a hard-template-assisted strategy as an oxygen reduction catalyst for Al-air batteries

Kun Liu [a], Ke Hu [a], Nannan Zhang [a], Yujing Ling [a], Xianglong Guan [a], Taotao Xu[a], Angli Zhang [a], Jing Wang [a], Xiaowu Liu [a*], Xucheng Fu [b*]

[a] *Anhui Provincial Laboratory of Biomimetic Sensor and Detecting Technology, College of Materials and Chemical Engineering, West Anhui University, Lu'an 237012, Anhui Province, China.*

[b] *Analytical and Testing Center, West Anhui University, Lu'an 237012, Anhui Province, China*

The Koutecky-Levich diagram (J^{-1} vs $\omega^{-1/2}$) was investigated under different electrode potentials. In accordance with the Koutecky-Levich equation, the electron transfer number (n) can be determined by calculating the slope of its linear regression line. The hydrodynamic properties of the prepared sample can be evaluated using the following Koutecky-Levich equation:[1]

$$\frac{1}{j}=\frac{1}{j_L}+\frac{1}{j_K}=\frac{1}{B\omega^{1/2}}+\frac{1}{j_K} \quad \text{Equation (1)}$$

$$B=0.62nFC_0D_0^{2/3}\upsilon^{-1/6} \quad \text{Equation (2)}$$

For the Tafel plot, the kinetic current was calculated as equation (3):

$$j_K=\frac{j\times j_L}{j_L-j} \quad \text{Equation (3)}$$

The experimentally measured current density, denoted as j, is compared to the diffusional-limited current density (j_L) and dynamic current density (j_K). The electrode

speed is represented by ω in rad·s^{-1}. F refers to the Faraday constant (96485 C·mol^{-1}), while C_0 (1.2 ×10^{-3} mol·L^{-1}) and D_0 (1.9 ×10^{-5} cm^2·s^{-1}) correspond to the volume concentration and diffusion coefficient of O_2 in 0.1 M KOH respectively. ν represents the kinematic viscosity of the electrolyte with a value of 0.01 cm^2·s^{-1}. B denotes the K-L graphs.

The rotating ring disk electrode (RRDE) technique was estimated transfer number (n). The equation provided both the electron transfer number (n) and the yield of hydrogen peroxid (%H_2O_2) from the following equations (4-5):[2]

$$\%HO_2^- = 200 \times \frac{I_r / N}{I_d + I_r / N} \quad (4)$$

$$n = 4 \times \frac{I_d}{I_d + I_r / N} \quad (5)$$

Where Id represents disk current, Ir represents ring current, and N represents current collection efficiency of the Pt ring (0.424).

The electrochemical surface area (ECSA) of the prepared catalyst was assessed through cyclic voltammetry (CV) in a non-rotating N_2-saturated 0.1M KOH electrolyte. CV curves were recorded for RDE working electrodes at various scanning rates (1, 5, 7，10, 15, and 25 mV/s) within the non- faradic potential range of 1.00~1.10V relative to RHE. Subsequently, a scatter plot was generated depicting the average current density (ΔJ/2, ΔJ = Ja-Jc, mA/cm^2) against sweep rate (mV/s) at 1.05V. The slope obtained from linear regression analysis between ΔJ/2 and scan rate corresponds to the differential capacitance value (C_{dl}, mF/cm^2), which is directly proportional to ECSA and can be utilized for comparing ECSA among different materials，ECSA = $\frac{C_{dl}}{C_s}$, the ECSA can be calculated. Here, C_s = 0.04 mF/cm^2, which is the speciffc capacitance.[3,4]

Fabrication and performance evaluation of Al-air batteries.

The air electrode consists of three layers: a catalytic layer, a fluid collector layer, and a gas diffusion layer. The positive electrode of the air electrode is then obtained through hot pressing method. Aluminum-air battery is formed by assembling the positive electrode material with the negative electrode made of aluminum plate and electrolyte, allowing for the study of electrochemical activity in the catalyst within the positive electrode. Nickel foam, known for its excellent electrical conductivity and high strength, serves as an ideal fluid collector for air electrodes. The catalyst layer is prepared by mixing catalyst, acetylene black, Ketjenblack, and polytetrafluoroethylene (PTFE) in a weight ratio of 3:1:3:3. This mixture is dispersed into a uniform slurry using ethanol. Once it reaches paste consistency, it is rolled onto a glass plate until it forms a thickness of approximately 0.2 mm. The air electrode thickness was compressed to the range of 0.3-0.5mm (3 cm×5 cm) using the roller press (MSK-HRP-MR100A) provided by Hefei Kejing. Finally to vacuum drying at 60°C for a duration of 12 hours. During the entire battery test, the air electrode are used as the cathode while the polished aluminum electrode functioned as the anode electrodes. A corrosion inhibitor electrolyte consisting of 6mol·L^{-1} KOH, 0.0005mol·L^{-1} $In(OH)_3$, 0.0075mol·L^{-1} ZnO and 0.01mol·L^{-1} Na_2SnO_3 was employed.The constant discharge test was carried out on the Neware battery test system (Shenzhen, China) using the aluminum air battery test device of Youkete New Energy Technology Co., LTD. (OMS-TF1) (Changzhou, Jiangsu, China). The detailed experimental procedures have been described in our previous work.[5]

Supporting Figures

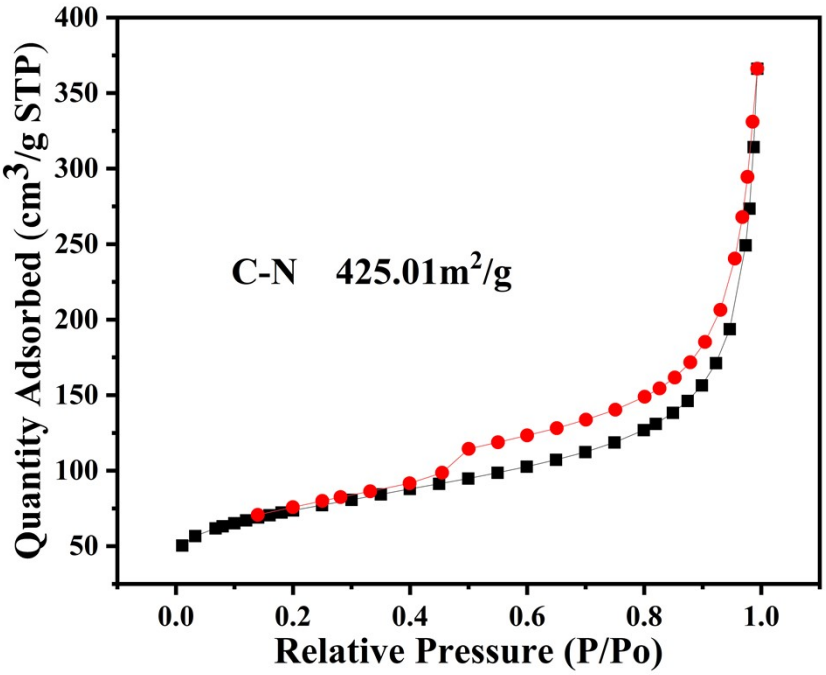

Figure S1. N_2 adsorption-desorption isotherms of C-N catalyst.

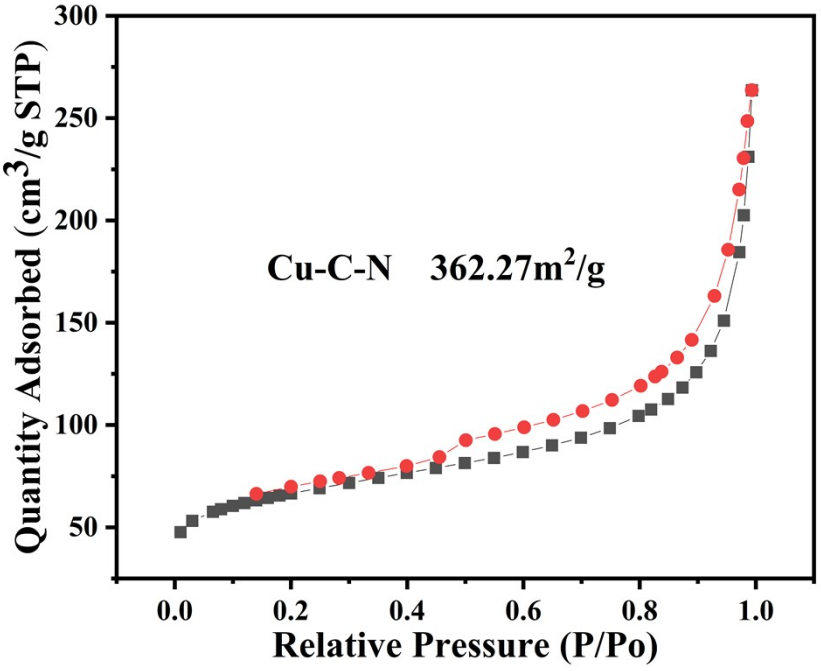

Figure S2. N_2 adsorption-desorption isotherms of Cu-C-N catalyst.

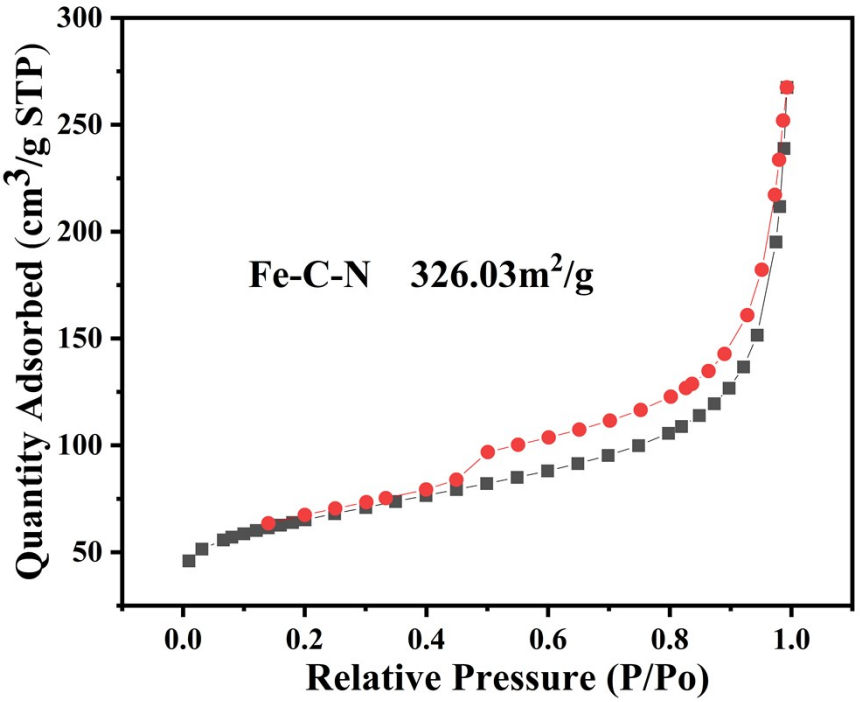

Figure S3. N_2 adsorption-desorption isotherms of Fe-C-N catalyst.

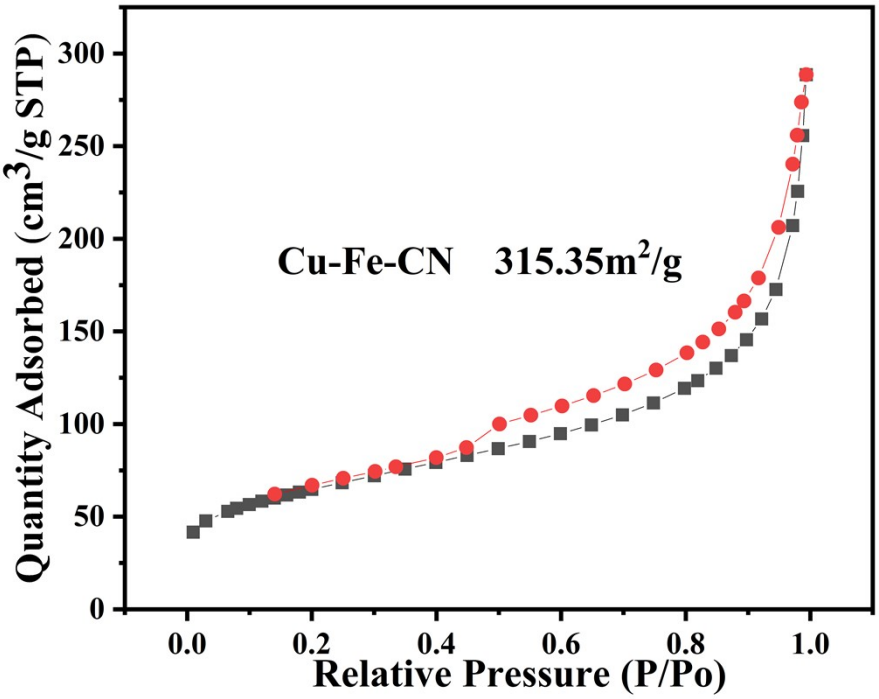

Figure S4. N_2 adsorption-desorption isotherms of Cu-Fe-CN catalyst.

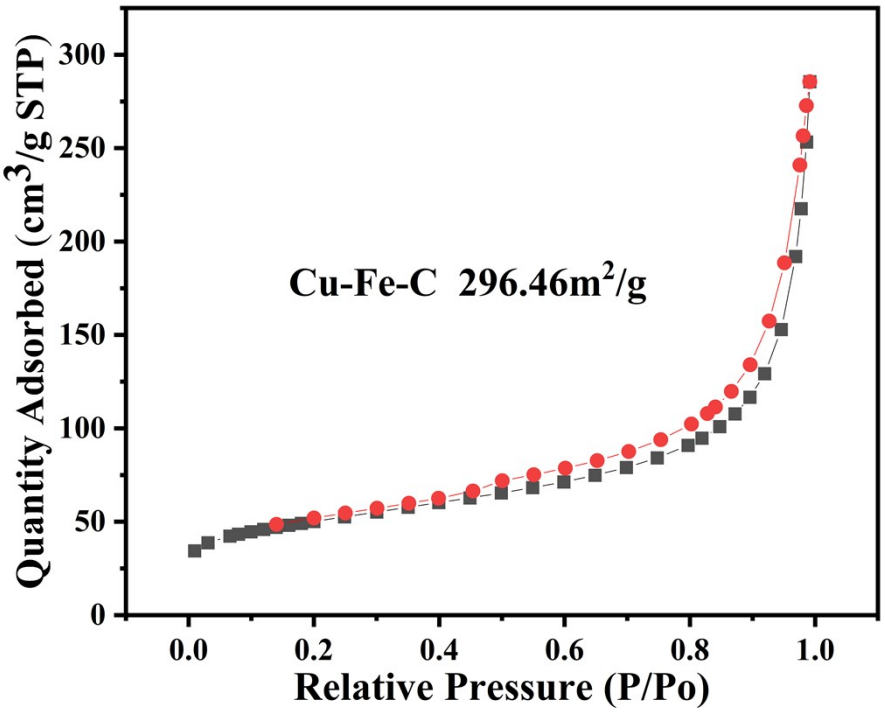

Figure S5. N_2 adsorption-desorption isotherms of Cu-Fe-C catalyst.

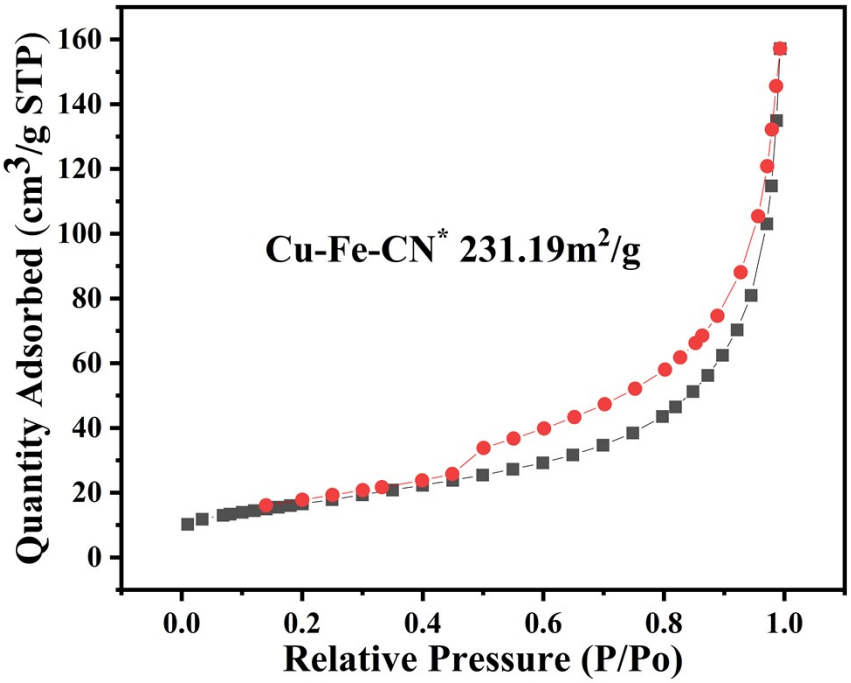

Figure S6. N_2 adsorption-desorption isotherms of Cu-Fe-CN* catalyst.

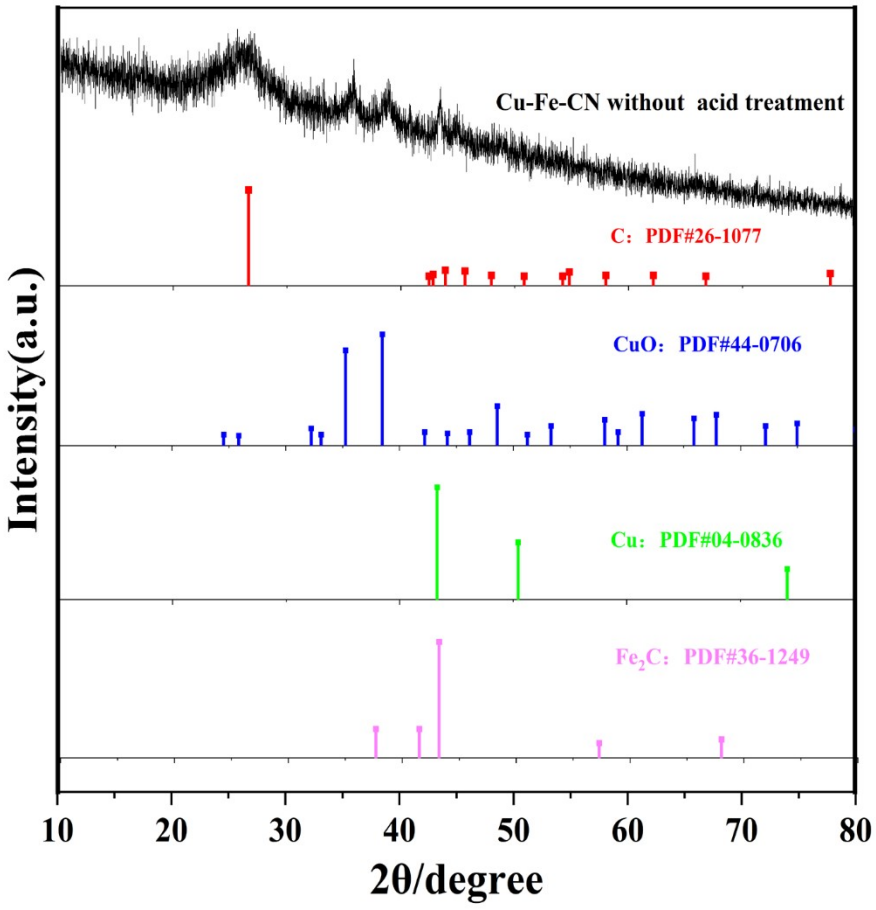

Figure S7. XRD patterns of Cu-Fe-NC without acid treatment.

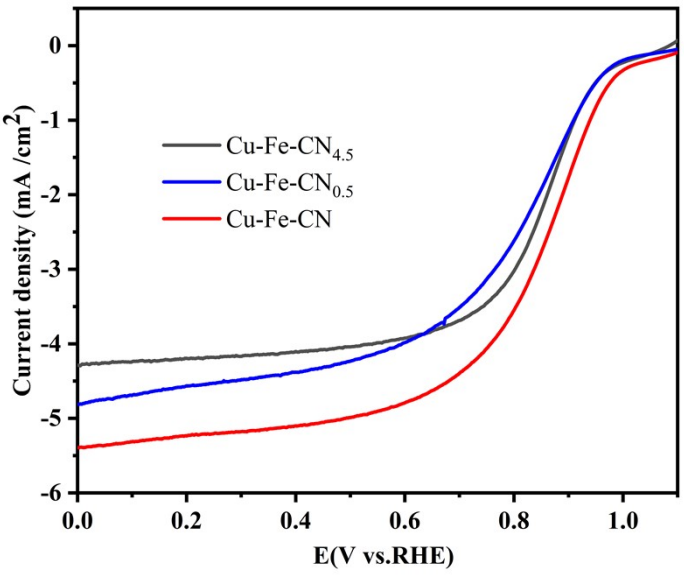

Figure S8. LSV curves of Cu-Fe-$CN_{0.5}$, Cu-Fe-CN, and Cu-Fe-$CN_{4.5}$ in O_2-saturated 0.1 M KOH solutions with a rotation speed of 1600 rpm.

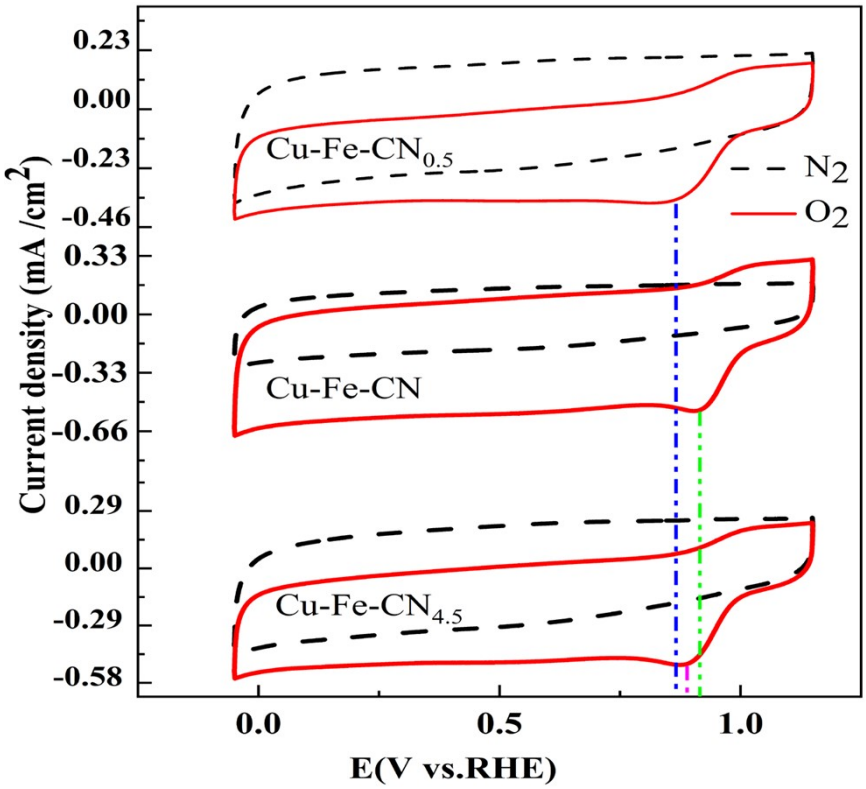

Figure S9. CV curves of different samples for different dicyandiamide addition amount in O_2-saturated (solid line) and N_2-saturated (dash line) 0.1 M KOH solutions.

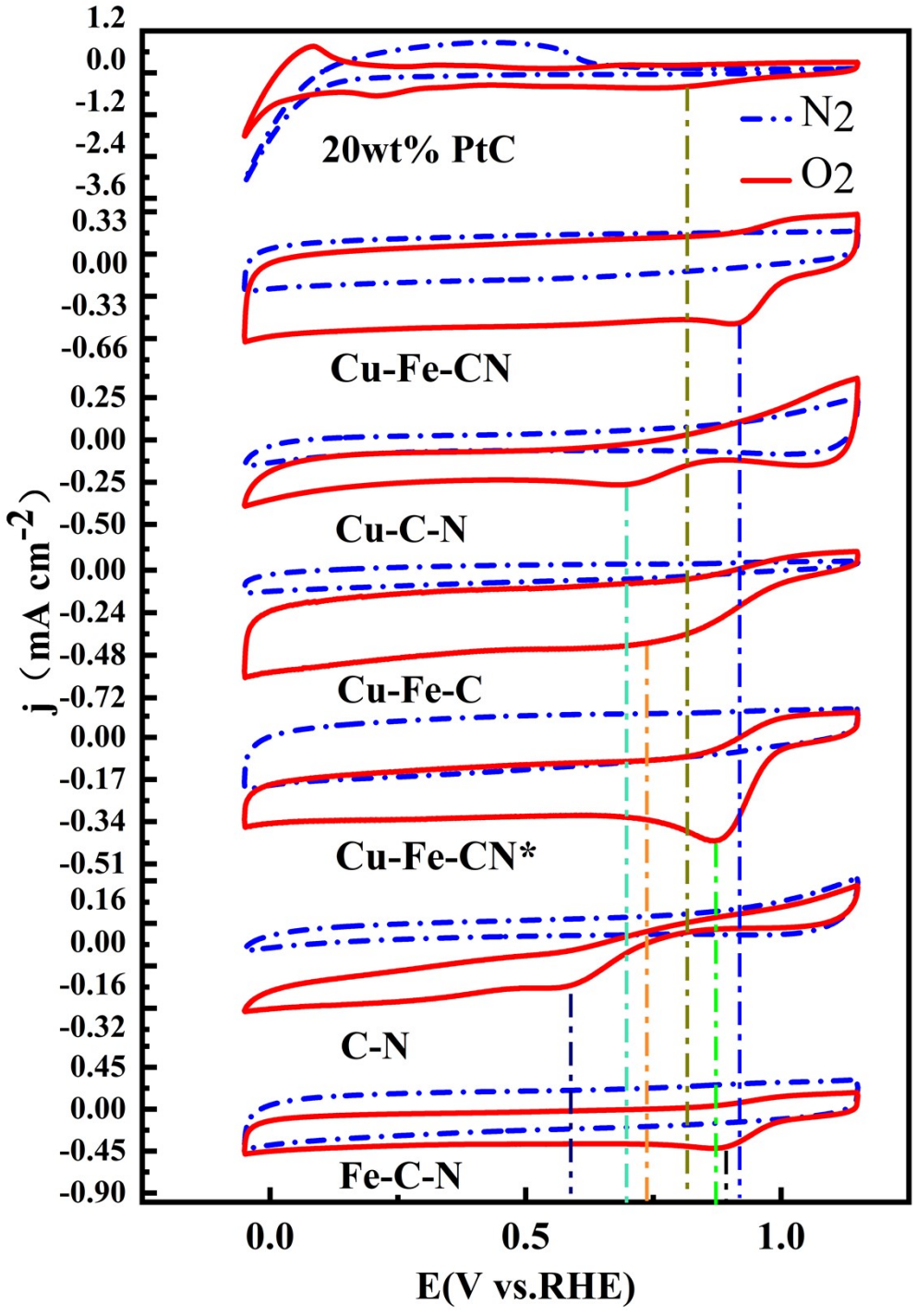

Figure S10. CV curves of different samples in O_2-saturated (solid line) and N_2-saturated (dash line) 0.1 M KOH solutions.

.

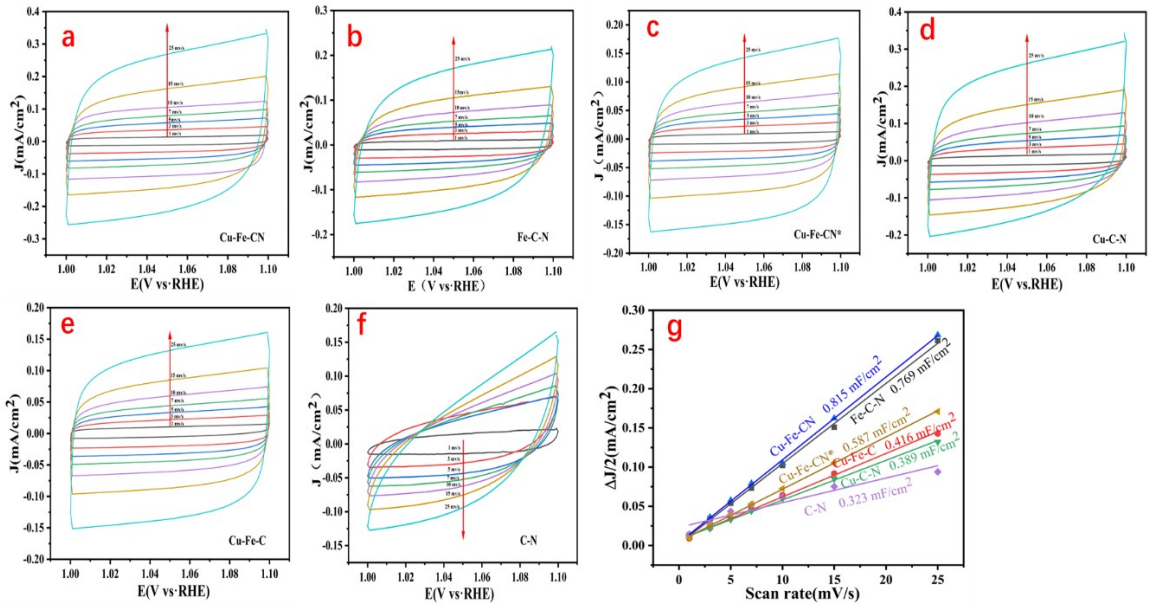

Figure S11. The CV curves for (a) Cu-Fe-CN, (b) Fe-C-N, (c) Cu-Fe-CN*, (d) Cu-C-N, (e) Cu-Fe-C, and (f) C-N at different scan rates in N_2-saturated 0.1 M KOH solution, (g) Capacitive current density against scan rate.

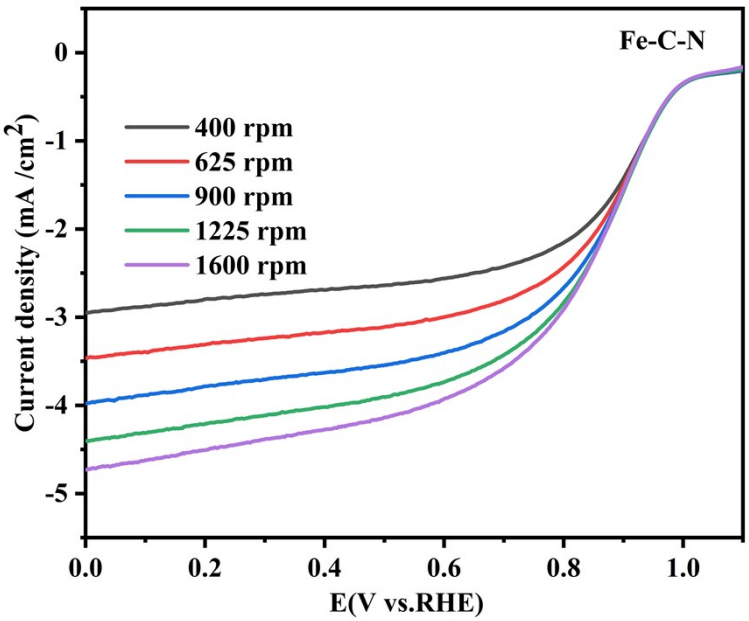

Figure S12. LSV curves of Fe-C-N at different rotation rates.

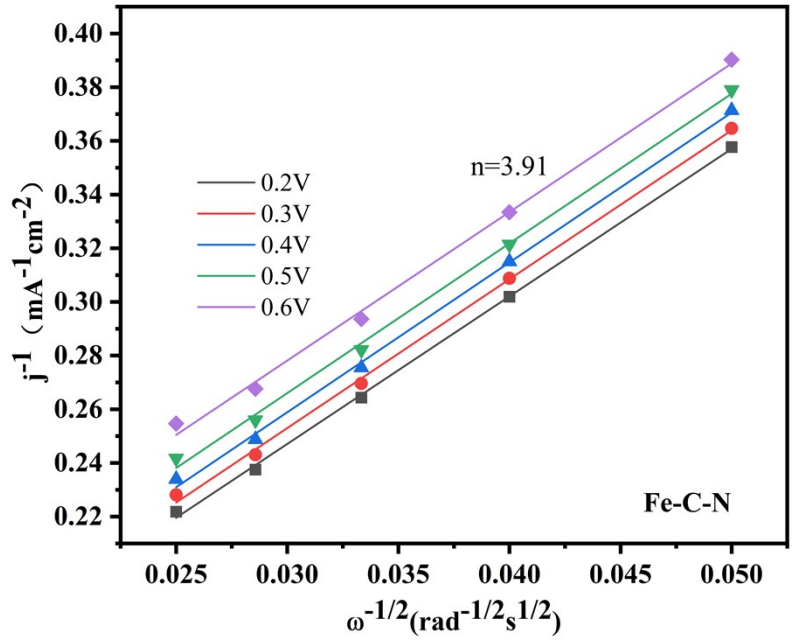

Figure S13. Koutecky-Levich (K–L) plots for Fe-C-N at different potentials.

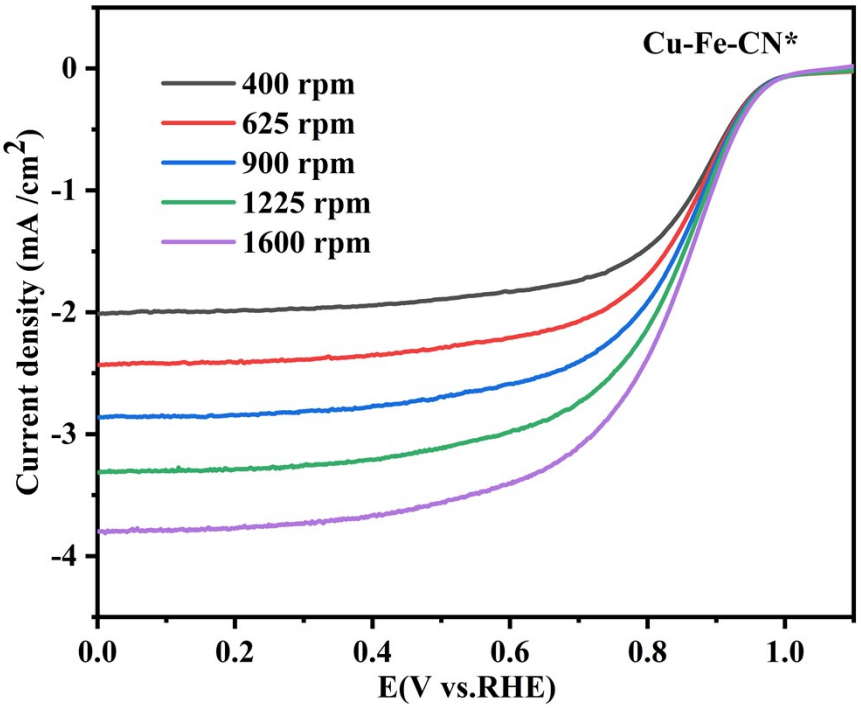

Figure S14. LSV curves of Cu-Fe-CN* at different rotation rates.

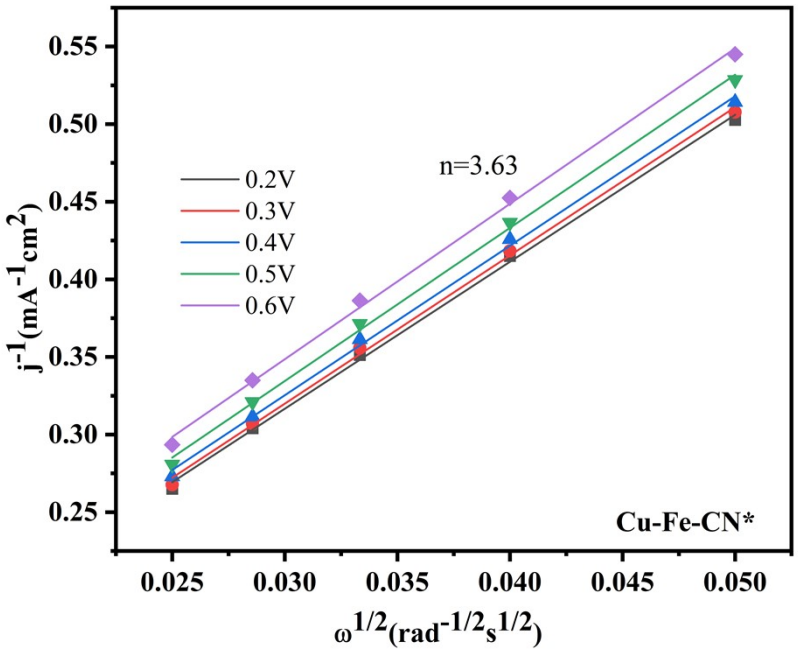

Figure S15. LSV curves of Cu-Fe-CN* at different rotation rates.

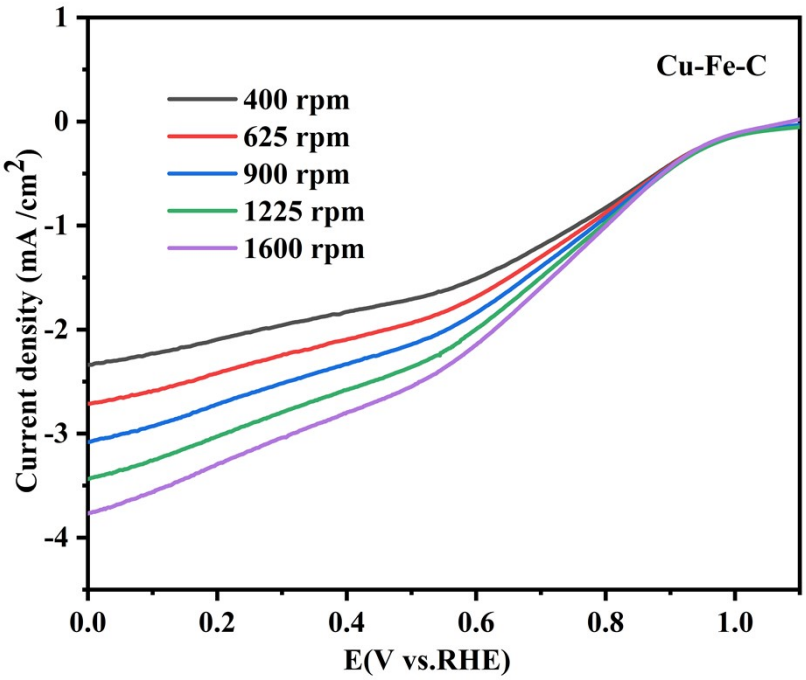

Figure S16. LSV curves of Cu-Fe-C at different rotation rates.

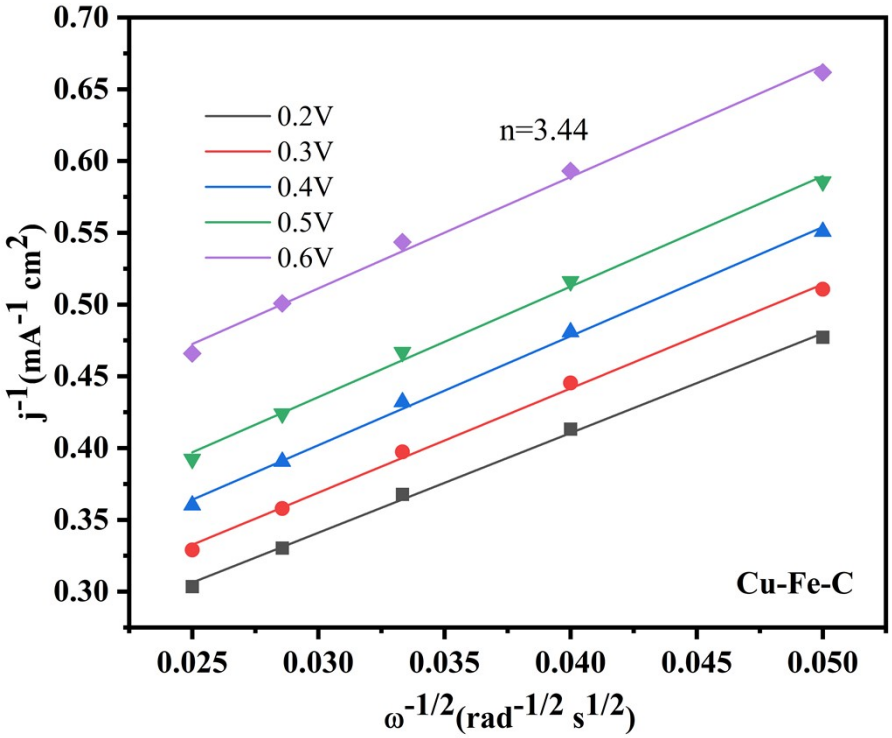

Figure S17. Koutecky-Levich (K–L) plots for Cu-Fe-CN* at different potentials.

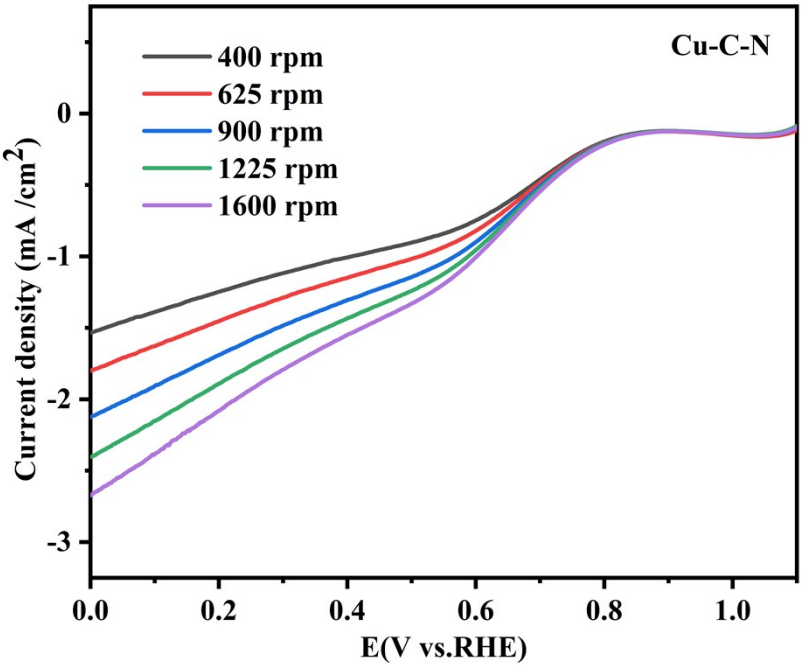

Figure S18. LSV curves of Cu-C-N at different rotation rates.

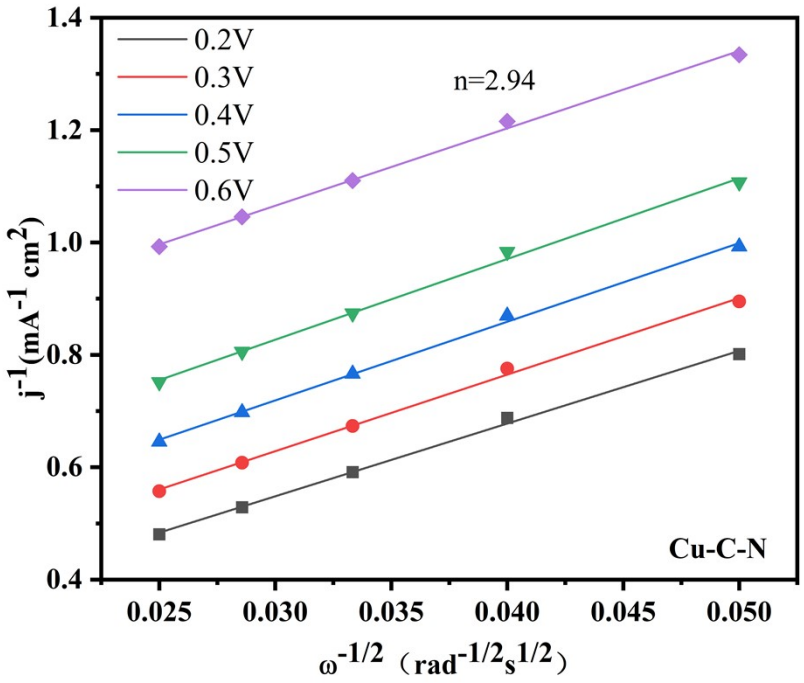

Figure S19. Koutecky-Levich (K–L) plots for Cu-C-N at different potentials.

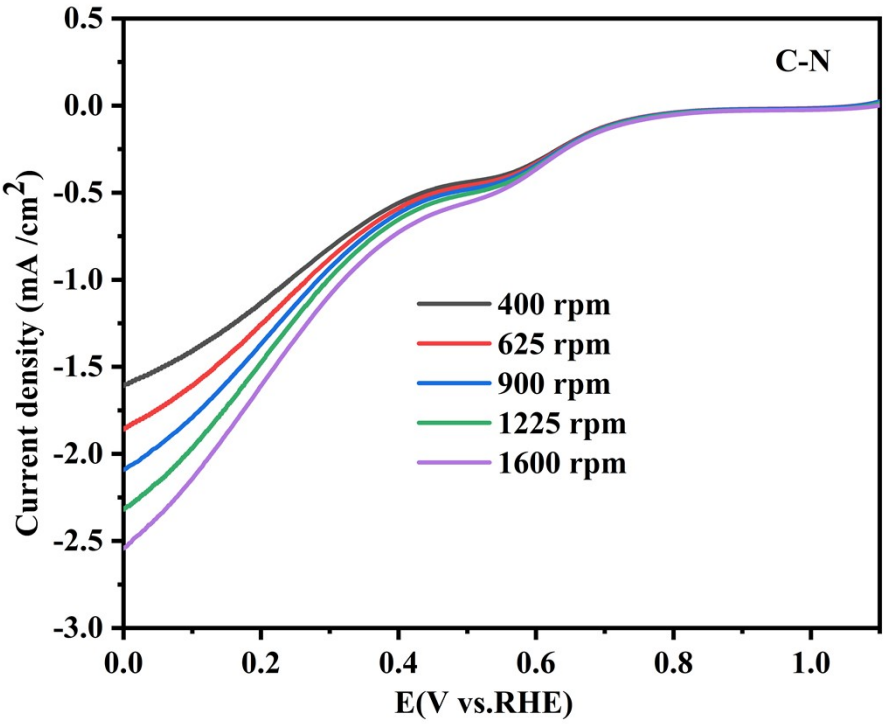

Figure S20. LSV curves of C-N at different rotation rates.

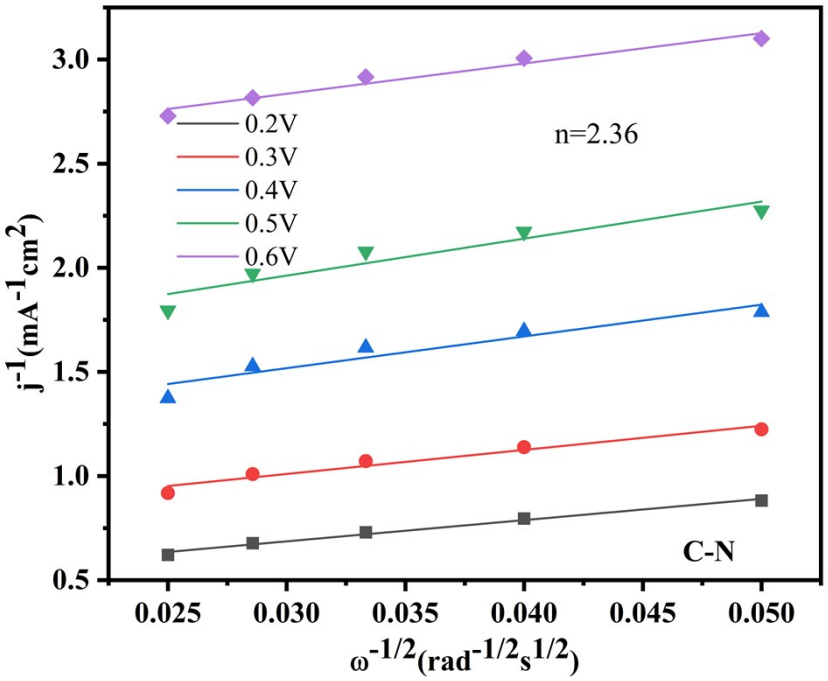

Figure S21. LSV curves of C-N at different rotation rates.

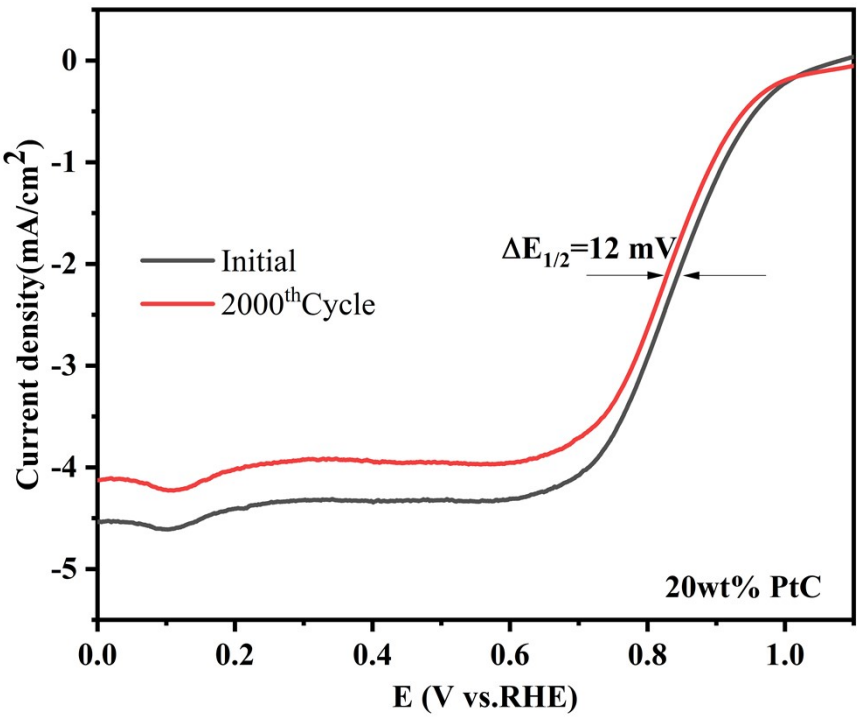

Figure S22. The ORR activity of 20 wt % Pt/C, measured before and after 2000 cycles.

References

1 J. Li, J. Chen, H. Wan, J. Xiao, Y. Tang, M. Liu and H. Wang, Applied Catalysis B: Environmental, 2019, **242**, 209-217.

2. S. Zhang, Y. Wang, Y. Li, M. Wei and K. Wang, ACS Applied Energy Materials, 2022, **5**, 15909-15917.

3. Q. Lai, K. Wei, Z. Tang, X. Liu, J. Zheng and Y. Liang, Journal of Materials Science, 2021, **56**, 19577-19588.

4. K. K. Hazarika, Y. Yamada, E. V. Matus, M. Kerzhentsev and P. Bharali, Journal of Power Sources, 2021, **490**, 229511-229521.

5. K. Liu, X. Ye, A. Zhang, X. Wang, T. Liang, Y. Fang, W. Zhang, K. Hu, X. Liu and X. Chen, RSC Advance, 2024, **14**, 5184-5192.